JOC The Journal of Organic Chemistry

ARTICLE

pubs.acs.org/joc

On the Structure and Dynamics of Duplex GNA

Andrew T. Johnson,[†] Mark K. Schlegel,[‡] Eric Meggers,[*,‡] Lars-Oliver Essen,[*,‡] and Olaf Wiest[*,†,§]

[†]Department of Chemistry and Biochemistry, University of Notre Dame, Notre Dame, Indiana 46556-5670, United States

[‡]Fachbereich Chemie, Philipps-Universität Marburg, Hans-Meerwein-Strasse, 35032 Marburg, Germany

[§]School of Chemical Biology and Biotechnology, Peking University, Shenzhen Graduate School, Shenzhen 518055, China

Supporting Information

ABSTRACT: Glycol nucleic acid (GNA), with a nucleotide backbone comprising of just three carbons and the stereocenter derived from propylene glycol (1,2-propanediol), is a structural analog of nucleic acids with intriguing biophysical properties, such as formation of highly stable antiparallel duplexes with high Watson−Crick base pairing fidelity. Previous crystallographic studies of double stranded GNA (dsGNA) indicated two forms of backbone conformations, an elongated M-type (containing metallo-base pairs) and the condensed N-type (containing brominated base pairs). A herein presented new crystal structure of a GNA duplex at 1.8 Å resolution from self-complementary 3′-CTC^{Br}UAGAG-2′ GNA oligonucleotides reveals an N-type conformation with alternating gauche−anti torsions along its (O3′−C3′−C2′−O2′) backbone. To elucidate the conformational state of dsGNA in solution, molecular dynamic simulations over a period of 20 ns were performed with the now available repertoire of structural information. Interestingly, dsGNA adopts conformational states in solution intermediate between experimentally observed backbone conformations: simulated dsGNA shows the all-gauche conformation characteristic of M-type GNA with the higher helical twist common to N-type GNA structures. The so far counterintuitive, smaller loss of entropy upon duplex formation as compared to DNA can be traced back to the conformational flexibility inherent to dsGNA but missing in dsDNA. Besides extensive interstrand base stacking and conformational preorganization of single strands, this flexibility contributes to the extraordinary thermal stability of GNA.

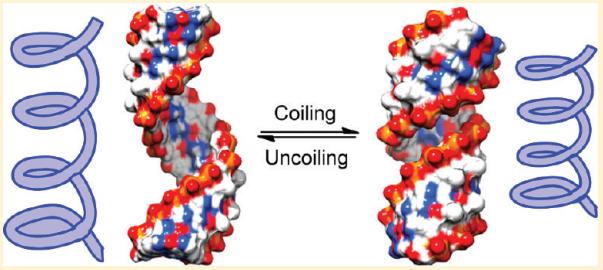

INTRODUCTION

For about the last 20 years, synthetic organic chemists have extensively modified the structure of DNA and RNA oligonucleotides to alter either their properties, e.g., for antisense technology, or to learn about the principles of genetic information storage and retrieval. The initial model of nucleic acid structure dating back to Watson and Crick[1] emphasized the importance of stacking the hydrophobic nucleobases in combination with specific hydrogen bonds within the base pairs A:T and G:C. Today, we know that the (deoxy)ribose phosphate backbone is not just a simple connecting unit for the nucleobases but is in fact crucial for duplex structure and stability. Many backbone replacements have been explored but, unexpectedly, only a few have been found to match or improve the duplex stability compared to natural DNA or RNA. Simplified acyclic (deoxy)ribose analogs are especially appealing from a synthetic perspective and as potential building blocks for primitive genetic molecules during the evolution of life on Earth.[2] Previous experiments with acyclic nucleotides in DNA revealed that adding one or more acyclic nucleotides to oligodeoxynucleotides resulted in strong thermal duplex destabilizations. This was attributed to lacking conformational preorganization of the more flexible acyclic nucleotides in single strands resulting in a significant entropic penalty upon duplex formation.[3−8]

Pioneering work from the Eschenmoser laboratory on the chemical etiology of nucleic acid structure[9] resulted in the discovery of nucleic acids derived from a tetrose sugar backbone that is capable of forming stable duplexes in an antiparallel fashion.[10] Such L-α-threofuranosyl oligonucleotides (TNA) demonstrated for the first time that the "six-bonds-per-backbone rule"[11] can be violated by having just five bonds in an arrangement of vicinal phosphodiester groups instead. Encouraged and inspired by Eschenmoser's TNA, we envisioned that the removal of the 4′-CH_2O group of TNA would result in a much simplified acyclic propylene glycol backbone. Indeed, such simplified glycol nucleic acids (GNA), shown in Scheme 1, form highly stable antiparallel duplexes in a Watson−Crick fashion which surprisingly surpass the thermal and thermodynamic stabilities of the analogous duplexes of DNA and RNA.[12] Interestingly, the *R*- and *S*-enantiomers, (*R*)-GNA and (*S*)-GNA, do not cross-pair with each other.[13] Thus, GNA uniquely combines atom economy with structural simplicity and high duplex stability. It constitutes the simplest scaffold for a chemically stable phosphodiester-bond-containing nucleic acid backbone. Given the combination of structural simplicity, straightforward synthetic accessibility, and

Received: July 15, 2011
Published: August 12, 2011

high duplex stability of GNA duplexes, GNA comprises a promising nucleic acid scaffold for applications in biotechnology and nanotechnology and reinforces its candidacy as one of the initial genetic molecules formed during the origins of life on Earth.[14]

Two recently determined crystal structures of (*S*)-GNA homoduplexes, an 8-mer duplex containing two Cu(II)-coordinated hydroxypyridone homobase pairs (8-mer-CuGNA)[15] and a brominated 6-mer duplex (6-mer-BrGNA),[16] revealed that the overall GNA double helix differs significantly from canonical A- and B-form nucleic acids. Although it shares some similarities with RNA, it might be best described as a helical ribbon loosely wrapped around the helix axis (Figure 1a,b; see Table 1 for sequences and abbreviations). Within the backbone, the propylene glycol nucleotides can adopt two different conformations, gauche (in this paper gauche refers to the g-conformation) and anti, with respect to the torsional angles formed by O3′−C3′−C2′−O2′ (Figure 1d). A strikingly large tilt of the backbone with respect to the helical axis is present which results in extensive, zipper-like interstrand interactions and reduced intrastrand base−base interactions (Figures 1a−c and S8, Supporting Information, for a comparison with DNA). Interestingly, the two modified GNA structures display significant differences among each other that may or may not be a consequence of the different chemical modifications introduced into the duplex for phasing the crystallographic data. First, the 6-mer-BrGNA duplex is considerably compressed along the *z*-axis relative to the 8-mer-CuGNA. Although this compression is accompanied by very little change in the helix diameter, it causes the 6-mer-BrGNA to adopt a significantly shorter helical pitch of 26 Å with 10 residues per turn, in comparison to 60 Å with 16 residues per turn for the 8-mer-CuGNA helix. This shorter helical pitch results from the much stronger twist in the 6-mer-BrGNA, which subsequently brings the phosphate groups of opposing strands in closer contact. Second, the conformations of the propylene glycol backbone differ, especially the torsional angles between the vicinal C3′−O and C2′−O bonds. In the 6-mer-BrGNA duplex structure, the nucleotides adopt strictly alternating gauche and

Scheme 1. Constitutions of DNA, RNA, TNA, and the *S*- and *R*-Enantiomers of GNA

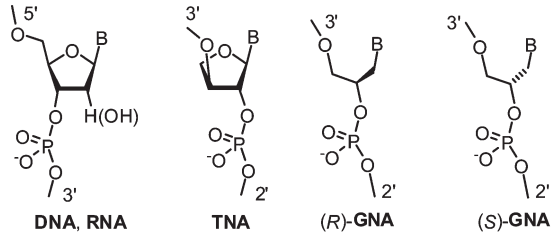

Table 1. List of Abbreviations and Sequences Used throughout the Paper[a]

6-mer-BrGNA	3′-G^{Br}CGCGC-2′
8-mer-BrGNA	3′-CTC^{Br}UAGAG-2′
16-mer-BrGNA	3′-CTC^{Br}UAGAGCTC^{Br}UAGAG-2′
8-mer-GNA	3′-CGAATTCG-2′
16-mer-GNA	3′-CGAATTCGCGAATTCG-2′
8-mer-CuGNA	3′-CGHATHCG-2′
16-mer-CuGNA	3′CGHATHCGCGHATHCG-2′
8-mer-DNA	5′-CGAATTCG-3′
16-mer-DNA	5′-CGAATTCGCGAATTCG-3′

[a] H = hydroxypyridone, ^{Br}C = 5-bromocytidine, ^{Br}U = 5-bromouracil.

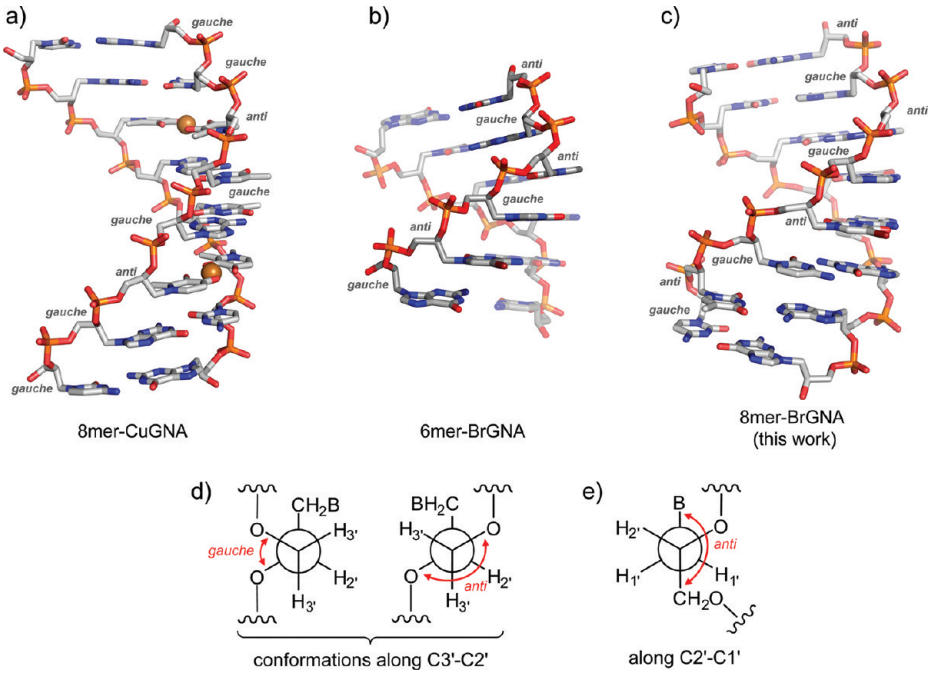

Figure 1. Crystal structures of (*S*)-GNA duplexes. (a) 8-mer-CuGNA derived from 3′-CGHATHCG-2′ (2JJA) in the presence of Cu^{2+}, with H = hydroxypyridone nucleobase. (b) 6-mer-BrGNA derived from 3′-G^{Br}CGCGC-2′ (2WNA), with ^{Br}C = 5′-bromocytosine nucleobase. (c) 8-mer-BrGNA derived from 3′-CTC^{Br}UAGAG-2′ (2XC6, this work), with ^{Br}U = 5′-bromouracil nucleobase. Gauche and anti refer to the torsional angles between the vicinal C2′−O and C3′−O bonds. (d) Newman projections of the gauche (g-) and anti conformations adopted by the torsional angle O3′−C3′−C2′−O2′. (e) Newman projection of the anti conformation adopted by the torsional angle N1−C1′−C2′−O2′.

dx.doi.org/10.1021/jo201469b |*J. Org. Chem.* 2011, 76, 7964–7974

anti conformations (type N), whereas in the 8-mer-CuGNA duplex structure the nucleotides forming conventional Watson−Crick base pairs adopt a gauche conformation (type M)[16] with respect to the torsional angles between C2′−O and C3′−O (Figure 1). In the latter, only the synthetic hydroxypyridone glycol nucleotides adopt anti conformations, presumably to compensate for the increased C1′−C1′ distance within the artificial metal base pair.

A recent report provides experimental insight into the origins of the high thermal stability observed for GNA.[17] Analysis of the thermodynamic parameters shows that while formation of GNA duplexes is less exothermic than its DNA counterpart, duplex formation is entropically not as costly for GNA. This surprising finding is counterintuitive considering that the GNA backbone is acyclic, consisting solely of rotatable bonds and would be expected to be much more flexible than the cyclic deoxyribose backbone. Loss of these degrees of freedom during duplex formation should therefore be entropically less favorable for GNA than for DNA, yet the opposite is observed. This could be due to the fact that single-stranded GNA (ssGNA) is less flexible than expected from its molecular structure, that GNA duplexes exhibit higher flexibilities than their DNA counterpart, or a combination of both. In the crystal structure of GNA, in both its duplex as well as single nucleotide form,[14] a strong preference is observed for the backbone to adopt an anti conformation with respect to the nucleobase (N1−C1′−C2′−O2′) (Figure 1e), while the vicinal C−O bonds (O3′−C3′−C2′−O2′) in single nucleotide crystal structures[16] favor a gauche conformation (Figure 1d). This, along with the presence of strong Cotton effects indicating the loss of helical structure in ssGNA upon heating, point toward preorganization of ssGNA prior to annealing as the main factor in the increased entropic stability in relation to DNA.

Molecular dynamics (MD) simulations of nucleic acids have significantly contributed to the understanding of structure and dynamics of both natural[18−22] and unnatural nucleic acids.[23−31] MD simulation can complement crystallography in the study of nucleic acids in a variety of ways. One obvious advantage is the ability to study species that do not lend themselves easily to crystallization. Second, MD simulations allow the investigation of the dynamics of a structure in the nanosecond time regime, whereas X-ray crystallography gives a snapshot for an otherwise time-averaged structure with little information about the underlying dynamics of the nucleic acid. Finally, in the absence of an experimental structure of unmodified GNA, model building and MD simulations can be used to understand the structure and dynamics of these interesting species.

In this paper, we present the first combined experimental and computational study of the structure and dynamics of parent GNA duplexes using different sequences and lengths (Table 1) to derive generalizable properties of GNA. We will start with a discussion of a new brominated 8-mer GNA (8-mer-BrGNA) duplex. With a GC content of 50% and six types of base steps, its sequence is more complex than the shorter 6-mer previously disclosed that comprised only repetitive GC and CG base steps. This will then, together with the recently determined structures of the Cu(II)−hydroxypyridone homobase-pairs-containing GNA duplex (8-mer-CuGNA) and the brominated 6-mer GNA (6-mer-BrGNA), serve as a starting point for the modeling of parent GNA (containing only natural nucleobases) and to deconvolute the effects of modifications that were introduced to phase their crystal structures by SAD and MAD techniques. The structure and dynamics of the GNA models are then compared with those from regular B-DNA to investigate backbone conformations of GNA and to rationalize the counterintuitive thermodynamic parameters that have been observed for GNA.

Table 2. Crystallographic Data and Refinement Statistics of 8-mer-BrGNA Duplex (3′-CTC^{Br}UAGAG-2′, 2XC6)

data collection statistics	
wavelength (Å)	0.919 85
resolution (Å)	15.8−1.83
space group	$I4_122$
completeness (%)	99.0 (98.3)
redundancy	17.4 (17.9)
R_{merge} [a,b]	0.054 (0.571)
$I/\sigma(I)$ [a,c]	32.2 (8.9)
B_{wilson} (Å^2)	34.2
refinement statistics	
resolution (Å)	8.00−1.83
R-factor/R_{free} [d]	0.234/0.271
average B-factor (Å^2)	26.6
water molecules	20
rmsd bonds (Å)	0.011
rmsd angles (Å)	1.715

[a] Values in parentheses correspond to the highest resolution shell. [b] $R_{merge} = ((\Sigma\Sigma|I_j(h) - \langle I(h)\rangle|/(\Sigma\Sigma I_j(h))$. [c] As calculated with the program SCALA. [d] $R = \Sigma||F_o| - k|F_c||/\Sigma|F_o|$, with k as a scaling factor; R_{free} calculated with test set (7.1% of all data).

RESULTS AND DISCUSSION

Crystal Structure of an 8-mer GNA Duplex (8-mer-BrGNA). Previous work revealed significant structural differences between an 8-mer metallo-GNA duplex (8-mer-CuGNA, Figure 1a) that harbored a Cu(II)-bridged hydroxypyridone homobase pair and a 6-mer GNA duplex containing a 5-bromocytosine (Figure 1b). For example, the elongated double helix of the former required 16 residues per turn, whereas the latter was condensed to only 10 residues per turn. At this point, it is not clear if these observations giving rise to the classification as M- and N-type GNA duplexes[16] are caused by the unique interstrand metal-coordination implemented in 8-mer-CuGNA, sequence differences, or the ability of GNA to adopt multiple conformations that depend on crystal packing.

We hence determined a GNA crystal structure which had a different sequence and utilized here only a 5-bromouracil (^{Br}U) modification for phasing at the bromine edge by multiple anomalous dispersion (MAD). The self-complementary sequence 3′-CTC^{Br}-UAGAG-2′ gave rod-shaped tetragonal crystals in sitting drop setups after 2 weeks at 4 °C in 10% 2-methyl-2,4-pentanediol, 40 mM sodium cacodylate, pH 5.5, 20 mM cobalt hexamine, 40 mM LiCl, 20 mM $MgCl_2$. Crystals diffracted up to a resolution of 1.8 Å at the synchrotron and allowed structure solution by standard MAD techniques (Table 2). The refined GNA duplex structure contains one single strand, 19 H_2O molecules, and two sodium ions. Unlike in the two previous structures of GNA duplexes, no electron density was assigned to cobalt−hexamine complexes that were so far found to be essential for GNA crystallization by associating to the phosphate moieties of the GNA backbone.

Table 3. Comparison of Average Helical Parameters for GNA Duplex Structures to B-DNA and A-DNA[a]

	8-mer-BrGNA (N-type)	6-mer-BrGNA (N-type)	8-mer-CuGNA (M-type)	B-DNA	A-DNA
helical sense	right	right	right	right	right
residues per turn	10	10	16	10	12
helical pitch (Å)	29	26	60	34	34
helical rise (Å)[b]	2.9	2.6	3.8	3.4	2.9
x-displacement (Å)[c]	−5.8	−6.0	−5.4	0.1	−4.2
tilt (deg)[d]	0.0	0.5	0.0	−0.1	0.1
Roll (deg)[d]	3.6	6.4	−2.8	0.6	8.0
twist (deg)[d]	35.8	35.7	22.9	36	31
slide (Å)[d]	−3.2	−3.4	−3.4	0.2	−1.5
P−P distance (Å)[e]	5.5	5.4	5.4	7.0	5.9

[a] Data for GNA were calculated using the program CURVES (ref 12). Data for B- and A-DNA were taken from refs 10 and 11. [b] Global interbase pair parameter. [c] Global base pair-axis parameter. [d] Local interbase pair step parameters. [e] Average intrastrand P−P distances.

All bases form standard Watson−Crick hydrogen bonds with the 5-bromouracil nucleotides having no apparent distorting effect. While having a completely unrelated sequence, this new duplex structure (8-mer-BrGNA) shows strikingly similar helix parameters like the previous 6-mer-BrGNA (Table 3). The backbone around the vicinal C3′−O3′ and C2′−O2′ bonds adopts the strictly alternating gauche and anti conformations of N-type GNA[16] so that each base pair contains one nucleotide in the gauche and one in the anti conformation. As a consequence of the alternating O3′−C3′−C2′−O2′ torsions, the phosphate−phosphate distances within the same strand of the GNA backbone of 8-mer-BrGNA alternate between 5.79 Å (anti) and 5.17 Å (gauche); similar values were observed for the 6-mer-BrGNA structure (5.58 Å, 5.09 Å).

From the structural data of the two determined brominated duplexes with very different sequences, 3′-G^{Br}CGCGC-2′ versus 3′-CTC^{Br}UAGAG-2′, it can be concluded that N-type GNA duplexes with their highly twisted and alternating gauche−anti backbone conformations can be formed independent of their sequences. Interestingly, the GNA nucleotides adopting gauche backbone conformations were found to comprise exclusively purine bases in the 6-mer-BrGNA with its track of alternating purine−pyrimidine nucleotides. In contrast, the new structure of the self-complementary 8-mer-BrGNA, where a stretch of four pyrimidine nucleotides is followed by four consecutive purine nucleotides, demonstrates that there is actually no intrinsic preference for purines to adopt gauche conformations. The lack of a specific backbone preference by GNA duplexes is corroborated by the copper(II)-containing duplex that adopts an all-gauche M-type conformation and is only disturbed at the Cu(II)-bridged hydroxypyridone base pair. Here, the C1′−C1′-distance (12.7 Å) is widened by about 2.0 Å as compared to standard Watson−Crick base pairs and triggers thereby at this position a change to the anti-conformation of the O3′−C3′−C2′−O2′ torsion. Overall, the crystal structures of GNA duplexes indicate a high variability of their backbone conformations that can currently not be traced back to unique interactions with counterions from the crystallization solution or restraints given by different packing arrangements.

MD Simulations of GNA Duplexes. To study the similarities and differences between GNA and its DNA counterparts, an understanding of the helicoidal parameters that describe their duplex structures is needed. Moreover, the ability of GNA duplexes to adopt gauche and anti conformations along their backbone in crystalline form needs analysis of their behavior in free solution, where context-free dynamics may indicate an intrinsic preference for backbone conformations. Using the structural information of the three different crystal structures of GNA duplexes, we performed 20 ns MD simulations for each (see Table S1 of the Supporting Information for system parameters). Additional starting structures for the simulation of longer GNA duplexes, which served as models for longer strands currently not experimentally accessible, were generated by linking symmetry-mates in the corresponding crystal structures, which we found to be already suitably packed in a quasi-continuous manner. The analysis of MD simulations was performed by writing the coordinates every 20 ps throughout the production run to obtain a total of 1000 snapshots. The coordinates of the non-natural nucleic acids were reformatted (scripts available in the Supporting Information) to generate input for a CURVES analysis of each structure. The results were averaged over all snapshots, and the helicoidal twist was plotted over time.

Analysis of MD Simulations Starting from N-type GNA Duplexes. Bromination of GNA bases in the two experimentally determined structures of 6-mer-BrGNA and 8-mer-BrGNA was not found to induce obvious perturbation of the GNA duplex structure, so that MD simulations could be directly based on the available structures. Table 4 lists the average value of helicoidal parameters obtained from both MD simulations as well as the used N-type GNA crystal structures. It can be seen that the results are in excellent agreement. For example, the local rise between neighboring base pairs remains almost unaffected by the simulation of GNA duplexes in solution as well as the base pair tilt and roll parameters. The only major difference here is the helical twist. It is not uncommon for solution simulations of nucleic acids to report different values for helical twist as well as several other backbone parameters due to the different environments caused by crystal packing. The crystallographic analysis of short oligonucleotides has the shortcoming of a high ratio of end-standing base pairs vs the number of base pairs in between. Accordingly, the end-to-end alignment of duplexes, often a prerequisite for the formation of ordered crystal lattices, needs some distortion of twist as compared to duplexes in free solution. It is also known that the AMBER force field tends to underestimate average base pair twist in DNA by ≈3°−4° and is also likely to factor in this observation.[32]

In the crystal structures the average helical twist is found to be ≈37° while in the MD simulation it is found to be 31.8° ± 2.4° and 30.9° ± 2.0° for the 6-mer- and 8-mer-BrGNA structures, respectively. The average base pair roll of the crystal structure is

Table 4. Average Helical Parameters for DNA and GNA Duplex Structures Obtained from Experiment and MD Simulations Starting from N-type Duplexes[a,b]

	8-mer-DNA			6-mer-BrGNA		8-mer-BrGNA		
	exp.	MD	16-mer-DNA MD	exp.	MD	exp.	MD	16-mer-BrGNA MD
shift (Å)[c]		0.1 (±0.2)	0.0(±0.2)	0.0	0.0(±0.2)	0.0	0.0(±0.2)	0.0(±0.1)
rise (Å)	3.4	3.5(±0.1)	3.5(±0.1)	3.2	3.3(±0.1)	3.3	3.3(±0.1)	3.3(±0.1)
tilt (deg)	−0.1	0.5(±1.9)	−0.7(±2.6)	0.0	0.0(±1.6)	0.0	0.2(±1.5)	0.1(±1.0)
roll (deg)	0.6	4.3(±2.8)	4.2(±2.3)	5.9	4.5(±2.8)	3.1	2.5(±2.9)	2.2(±1.6)
twist (deg)	36.0	32.9(±2.0)	33.3(±2.5)	37.2	31.8(±2.4)	36.8	30.9(±2.0)	30.6(±1.5)
slide (Å)	0.2	−0.6(±0.4)	−0.8(±0.3)	−3.3	−3.2(±0.3)	−3.2	−3.0(±0.3)	−3.0(±0.2)

[a] Data for nucleic acids were calculated using the program CURVES.[33,34] Data for B-DNA were taken from Olson et al.[35] [b] Standard deviations (in parentheses) given for MD data. [c] Local interbase pair parameters.

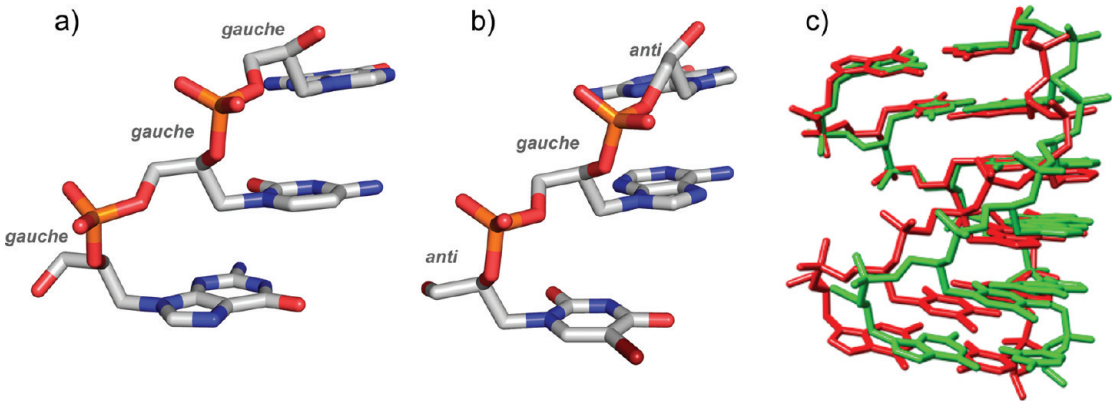

Figure 2. Comparison of backbone conformations of (a) the 16-mer-BrGNA MD with (b) the 6-mer-BrGNA crystal structure. (c) Overlay of the crystal structure of the 6-mer-BrGNA duplex (red) with the average structure from MD simulation (green). Anti and gauche refers to the torsional angle formed by O3′−C3′−C2′−O2′.

found to be approximately 1.4° higher than what is observed in the ensemble of molecular dynamics structures. An overlay of the crystal structure and average MD structure can be seen in Figure 2, showing the similarity of the structures with an average backbone rmsd of 1.4 Å. Apart from the average helical twist, the experimental and theoretical structures of 8-mer-BrGNA are also in excellent agreement.

One other major difference between the GNA duplex structures from crystals and MD simulations in solution is given by the significant conformational differences adopted by the O3′−C3′−C2′−O2′ backbone torsional angles. In the crystal structures of both the 6-mer- and 8-mer-BrGNA, this torsional angle is found to alternate between gauche and anti along the backbone. In the MD simulations, there is a strong preference for the gauche conformation and very few (less than 1%) structures adopt the anti conformation (Figure 2). Crystal structures of single GNA nucleotides show that the gauche conformation is indeed favored,[17] while the 8-mer-CuGNA structure shows a preference for the gauche conformation in areas away from the metal chelation site.[15] Close inspection of the crystal structures does not reveal any specific interactions that could rationalize the observed conformational behavior of the O3′−C3′−C2′−O2′ torsion. The possibility that it is caused by a combination of crystal packing and an accessible energy barrier concerning rotation about the C3′−C2′ bond needs therefore to be considered. Obviously the MD simulation of N-type GNA duplexes in solution allows a facile N→M transition of their backbone structures that is accompanied by a relaxed twisting of the overall duplex. The otherwise excellent agreement between the experimental and computed structures for 8-mer-BrGNA validates the approach chosen and makes a computational model building for parent GNA promising.

Analysis of MD Simulations Starting from Elongated M-type GNA Duplexes. We will continue the discussion with an analysis of the dsGNA crystal structure 8-mer-CuGNA that already adopts an M-type conformation in its crystalline state. Using this structure as a start point for MD simulations may give some indication whether the less twisted structure of the M-type duplexes obtained before by MD simulation of BrGNA duplexes is a feature of context-free behavior in solution or just one of various possibilities for GNA to adopt relaxed M-type structures. In addition, the two hydroxypyridone base pairs of 8-mer-CuGNA have to be considered which were engineered into the GNA strands to complex a copper ion.[15] While this metal−GNA hybrid allowed for the acquisition of the first GNA crystal structure, the interstrand complexation might not be representative of GNA duplexes containing only regular nucleobases. We hence studied the strands containing the hydroxypyridone base pairs as well as an analog where the two hydroxypyridone base pairs are replaced with A−T base pairs, resulting in the GNA sequence 3′-CGAATTCG-2′ (8-mer-GNA).

Overall, the helicoidal parameters provided by CURVES are quite similar between experimental and simulated CuGNA duplex structures.[33] The simulated CuGNA duplex structures

Table 5. Average Helical Parameters for GNA Duplex Structures Obtained from Experiment and MD Simulations Starting from M-type Duplexes[a,b]

	experiment		MD simulation			
	8-mer-CuGNA	16-mer-CuGNA[d]	8-mer-CuGNA	16-mer-CuGNA	8-mer-GNA	16-mer-GNA
shift (Å)[c]	0.0	0.0	−0.1(±0.2)	0.0(±0.1)	0.0(±0.2)	0.0(±0.1)
rise (Å)	3.5	3.4	3.5(±0.1)	3.5(±0.1)	3.5(±0.1)	3.4(±0.1)
tilt (deg)	0.0	0.0	−0.8(±1.6)	0.1(±0.9)	0.0(±1.5)	0.0(±2.2)
roll (deg)	−2.7	−2.8	−0.4(±2.4)	−2.4(±1.8)	0.9(±2.7)	1.2(±1.7)
twist (deg)	23.5	22.9	24.1(±1.9)	23.9(±1.6)	28.7(±2.2)	29.5(±1.4)
slide (Å)	−3.5	−3.4	−2.9(±0.2)	−2.9(±0.2)	−3.2(±0.3)	−3.5(±0.2)

[a] Data for nucleic acids were calculated using the program CURVES.[33,34] [b] Standard deviations (in parentheses) given for MD data. [c] Local interbase pair parameter. [d] 16bp−CuGNA created by including an additional asymmetric unit along the *z*-axis to create a quasi-continuous strand of twice the length.

remain in their elongated state with an almost unaffected twist of 24°, i.e. ∼15−16 base pairs are required per helix turn. In contrast, an exchange of the synthetic Cu(II)/hydroxypyridone base pairs against natural ones induces a significantly increased average twist between successive base pairs that is calculated to 29° ± 2.2° for the 8-mer-GNA MD simulation and 30° for the structural ensemble of the 16-mer-GNA simulation (Table 5). Accordingly, the latter M-type structures show a similar helical twist as observed before for BrGNA duplexes of ≈12 residues per turn. Apparently, the synthetic Cu(II)/hydroxypyridone base pairs, which make up 25% of all base pairs present in 8-mer-CuGNA, exert a strong unwinding effect on the overall GNA duplex structure. Interestingly, a similar effect of unwinding was recently observed in the NMR structure of a synthetic DNA hybrid which comprised three consecutive Ag(I)/imidazole base pairs. There the helical B-form DNA twist was reduced from 36° to ∼28°.[36]

A structural reason for the difference between M-type duplexes adopted by CuGNA and others is certainly the conformations adopted by the phosphate backbone. It can be seen in the crystal structure of CuGNA that the O2′−C2′−C3′−O3′ torsion belonging to the hydroxypyridone base pairs adopts an anti conformation that remains stable during MD simulations, while the same torsion belonging to natural base pairs adopts a gauche conformation. An obvious explanation is that the backbone is rather flexible and capable to convert rapidly between the gauche and anti conformations. In CuGNA the metallo−base pairs are stiffening the duplex structure to some extent so that it adopts the observed elongated form of ∼16 base pairs per turn. Taken together, these results indicate that duplex GNA with natural base pairs generally prefers to adopt a more condensed N-type backbone conformation of just 12 base pairs per turn.

However, another possibility for the obtained different helix turn heights and twists has been proposed by Darden and co-workers.[37] They observed that in MD simulations of duplex DNA, where the dimensions of the crystal lattice are fixed to the experimentally determined lattice size, the helicoidal parameters matched well. It should be noted that they used the Parm94 force field known to underestimate the B-DNA helical repeat comparing to the more recent Parm98/99 parametrizations. However, several differences could be discerned when comparing an unconstrained MDs simulation in solution and MD simulation of the crystal lattice. Most notably, the helicoidal parameters concerning backbone conformation as well as the helical twist parameters differed substantially between structural ensembles in solution and in the crystal lattice. The differences in the backbone torsional angles observed in our simulations and the X-ray structure match the results by Darden and co-workers and point to relatively strong effects of crystal packing on GNA duplex conformation. Finally, in the absence of accurate experimental solution structures of DNA or GNA addressing this point, incorrect force field parameters in both cases can, of course, not be excluded.

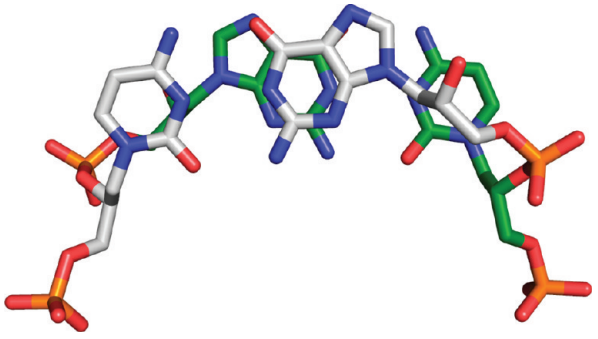

Figure 3. View of a 2′−2′ purine interstrand base stack in 16-mer-GNA.

Comparison of GNA and B-DNA Duplexes. With the success of using different forms of GNA crystal structures to perform model building and MD for generating undisturbed and converging dsGNA structures, a model of the elusive parent GNA structure containing only natural nucleobases can now be proposed on the basis of the 16-mer-GNA. As expected, the structures of dsDNA and dsGNA differ substantially. Most notably, the average base pair slide of GNA is calculated to be ca. −3.2 to −3.5 Å, whereas DNA possesses an average base pair slide of ca. −0.6 Å. This large difference causes GNA to base stack in an interstrand fashion as opposed to the conventional intrastrand base stacking seen in canonical dsDNA.[38] Hydrophobic overlap can be seen when a base stack contains two 2′-purines (Figure 3). These purine/purine contacts could help stabilize the GNA duplex. One of us had tested this hypothesis by using overhanging bases on either the 3′ or 2′ termini.[17] It was observed that overhanging nucleotides at the 2′-termini lead to strong stabilization of the duplex. The addition of overhanging adenines on the 2′-termini leads to an increase of melting temperature of 14.6 °C and an increased thermodynamic stability of 4.0 kcal mol^{-1}. This overlap of 2′-nucleobases is captured by all MD simulations presented, as indicated by the large, negative average base pair slide (−2.9 to −3.5 Å). When overhanging bases are added to the 3′-end, it results in only a slight increase in melting temperature (0−1.2 °C). Also, addition of nucleotide overhangs on DNA produced a less pronounced effect.

Table 6. Results from Normal Mode Calculations of Single- and Double-Stranded 16-mer-DNA and GNA[a]

	single stranded		double stranded		single strand − double strand	
	TS_{vib}	TS_{total}	TS_{vib}	TS_{total}	$T\Delta S_{vib}$	$T\Delta S_{total}$
DNA (ε = 4)	405.1	435.8	786.1	818.2	24.0	53.3
GNA (ε = 4)	361.4	391.9	705.2	737.1	17.6	46.6
DNA (ε = 80)	402.6	433.3	778.5	810.5	26.7	56.1
GNA (ε = 80)	354.6	384.8	687.7	719.2	21.4	50.3

[a] All results are in kcal mol^{-1}. ε denotes the dielectric constant used in the *nmode* calculations.

The simulations showed that dsGNA duplexes comprising only standard nucleobases combines structural elements from all experimental GNA structures. The average base pair slide of the BrGNA crystal structures is most similar to the simulated dsGNA structure by possessing an average base pair slide of −3.3 Å as compared to −3.2 Å. The average base pair roll of dsGNA is predicted to be a hybrid between the experimental structures possessing a roll of ≈0.9° compared to −2.7°, 5.9°, and 3.1° for the 8-mer-CuGNA, 6-mer-BrGNA, and 8-mer-BrGNA structures, respectively. dsGNA is expected to possess an average helical twist of ≈29° ± 2.2, which lies approximately halfway between the ≈23° helical twist found in the 8-mer-CuGNA and the ≈37° helical twist observed in the 8-mer-BrGNA crystal structures.

Dynamics of the GNA Duplex. In order to explore the relative entropic effects between DNA and GNA annealing, we performed frequency analysis to get a more quantitative information on the entropy from the simulations. Twenty nanosecond trajectories of 16-mer duplex and single stranded DNA and GNA were obtained, and 400 snapshots were taken from each trajectory and subjected to vibrational mode analysis using the *nmode* module of AMBER. Previous experimental work has shown that GNA incurs substantially less entropic penalty upon duplex formation in comparison to DNA (Table 6). The $\Delta\Delta S$ observed between DNA and GNA is ≈14 kcal mol^{-1}. Results obtained from vibrational analysis predict the $\Delta\Delta S$ between DNA and GNA to be ≈5.8−6.7 kcal mol^{-1}. In agreement with previous analyses of entropic contributions to dimerization,[39] the absolute magnitude of $\Delta\Delta S$ obtained using *nmode* is underestimated by ∼50%, possibly because the solvent molecules and counterions are not considered in the normal mode calculation. Nevertheless, the results clearly show that GNA duplex formation is entropically more favorable than in DNA. These calculations also suggest that the largest contribution to $\Delta\Delta S$ is due to vibrational entropy. This affirms the hypothesis that the observed twisting/untwisting motions present in dsGNA are likely responsible for the entropic effects previously explained. Another interesting observation is that in the simulations of ssGNA no hairpin formation occurs throughout the trajectory. Hairpin formation is typical of ssDNA[40] but is not observed in the 20 ns simulations of ssGNA. Therefore, the GNA single strand itself may not be as flexible as its DNA counterpart, contributing to the differences in entropic penalty observed between the two species. Of course, other possibilities such as solvation effects cannot be excluded, but they are beyond the scope of this study.

The analysis of the MD trajectories of dsGNA helps to rationalize the counterintuitive observation that duplex formation in GNA is entropically less unfavorable than for DNA[2] as well as the high stability of the GNA complexes. The results clearly show that the structure is quite flexible, as demonstrated by the rmsd plots of the backbone atoms (P, C2′, C3′, O2′, and O3′)

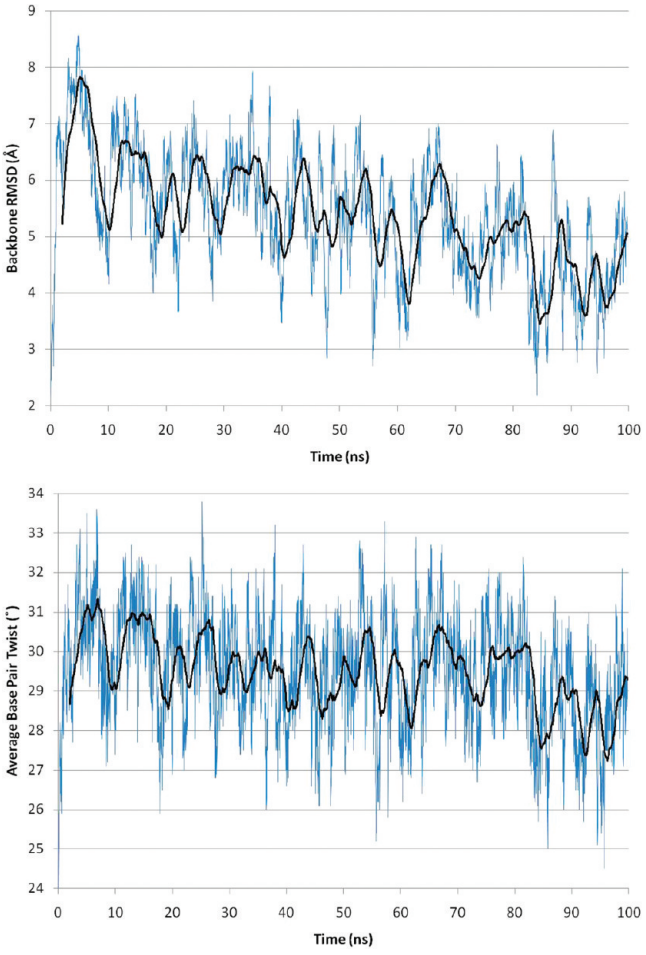

Figure 4. Backbone rmsd and average base pair twist versus time from the 16-mer-GNA simulation. The black curves highlight periodical variations and correspond to a moving average of fluctuations using a window size of 2 ns.

with periodic fluctuations on the 8−10 ns time scale for 16-mer-GNA, shown in Figure 4 (results for 8-mer-GNA are shown in the Supporting Information), which is associated with a helicoidal twisting and untwisting mode which is observed along the entire 100 ns trajectory. It is interesting to note that this motion is quasi-periodic with distances between the minima ranging from ∼5 to ∼15 ns. This is in line with the previously described function of DNA as a "molecular spring"[41] and suggests that GNA has an even larger amplitude of the twisting and untwisting mode. This conformational flexibility allows access to a large number of microstates for the backbone torsions and is consistent with the

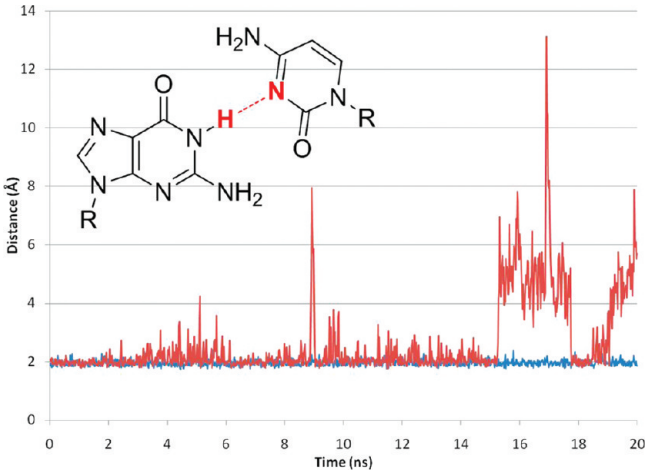

Figure 5. Plot of hydrogen-bond distance versus time of a terminal G-C base pair: red = DNA duplex, blue = GNA duplex. The hydrogen bond of interest is shaded red in the structure.

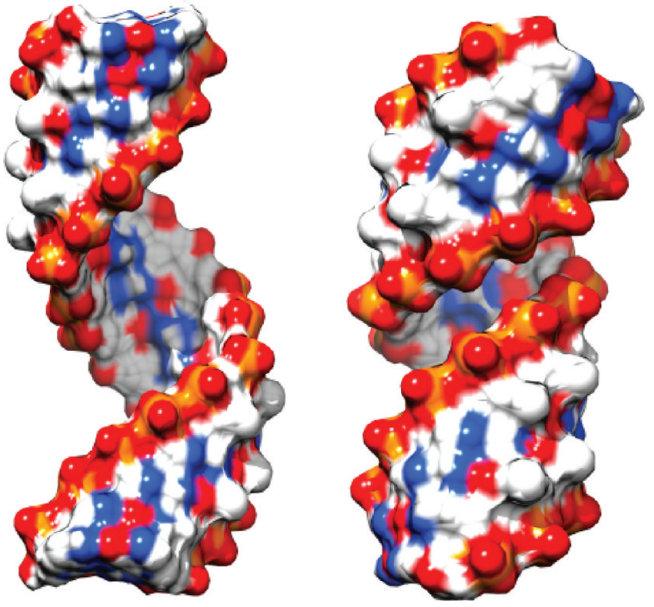

Figure 6. Uncoiled and coiled structures observed in the simulation of the 16-mer-GNA duplex.

decreased entropic penalty relative to dsDNA observed in the thermodynamic analyses of duplex formation. Although modes of dsDNA also have a significant degree of torsional plasticity,[42] including twisting and untwisting, the modes observed for dsGNA are quite different from that based on the large changes in the persistence length of the dsGNA and the winding and unwinding of the ribbon helix.

The MD trajectories may also shed light on the inherent stability found in dsGNA. While the backbone rmsd fluctuates throughout the simulation time, hydrogen bonding across the duplex remains intact for dsGNA (blue in Figure 5), but not for dsDNA (red in Figure 5). This indicates that much of the enthalpic contribution to duplex formation found in dsDNA is retained in the backbone while the ability of dsGNA to adopt variable backbone conformations leads to the increased entropy found for dsGNA formation. Accordingly, for dsDNA the duplex structure is more rigid and thermal energy tends to rupture hydrogen bonds and melting of the duplex. On the other hand, in GNA it appears that thermal energy leads to enhanced global molecular motions rather than the rupturing of hydrogen-bonded base pairs. The flexibility of the GNA backbone adapts to the thermal motion and resists duplex melting. While end-fraying effects cannot be used as a predictor of duplex melting, it is of note that with the enhanced molecular motions present in GNA that no end-fraying can be observed in our 100 ns simulation. These observations from the simulations are fully consistent with the experimental results suggesting a decreased entropic penalty for the formation of the GNA duplex.

CONCLUSIONS

The reported new crystal structure of a brominated 8-mer-GNA duplex, together with previous structures of a 6-mer-BrGNA duplex of different sequence and a copper(II)-hydroxypyridone base pair containing 8-mer GNA duplex, allow us to identify some general features of GNA duplexes. First, a large backbone-base inclination results in a significant slide between neighboring base pairs and thus the formation of extensive inter-strand base stacking. Second, the individual GNA nucleotides have the flexibility to adopt two different conformations with respect to the torsional angles between C2′−O and C3′−O. The alternating gauche−anti backbone observed in two brominated GNA duplexes lead to a highly twisted duplex and might constitute a general feature of GNA duplexes, although crystal packing effects cannot be ruled out.

The MD simulations of dsGNA explain the high duplex stability observed in duplex melting experiments through a combination of enthalpic and entropic factors. Backbone rmsd plots show periodic fluctuations that are associated with a twisting/untwisting mode while the enthalpic (hydrogen bonds and base stacking) contributions to free energy remain intact. This observation is consistent with the thermodynamic analyses put forth previously by one of us[17] and provides an explanation for the unique properties of dsGNA. While preorganization of ssGNA may play a part in the more entropically favorable duplex formation, the new finding of a twisting/untwisting mode inherent to duplex GNA (Figure 6) may additionally contribute to entropic stabilization. The flexible, yet energetically favorable nature of dsGNA is unique when compared to that of dsDNA. Most likely, dsGNA trades off base stacking in favor of an increased number of microstates leading to an overall increase in entropy. This increase in entropy more than makes up for what GNA loses in enthalpic contributions to free energy and hence generates a more stable and fluid structure than dsDNA. The MD simulations used in this work capture the main structural features found in the experimental structures. The major difference between the crystal structures and theoretical predictions is in the average helical twist that is affected by the gauche/anti distribution of the vicinal C−O backbone torsions. While the N-type crystal structures of BrGNA alternate between gauche and anti backbone configurations, the MD simulations show a strong preference for an all-gauche conformation that has previously been observed for the single-nucleotide GNA and double-stranded M-type CuGNA. In contrast to the latter, the relaxed form of M-type GNA structure has only 12 base pairs per turn and is significantly condensed. As stated above, this phenomenon is likely caused by the absence of disturbing metallo-base pairs and crystal packing artifacts that have been shown to

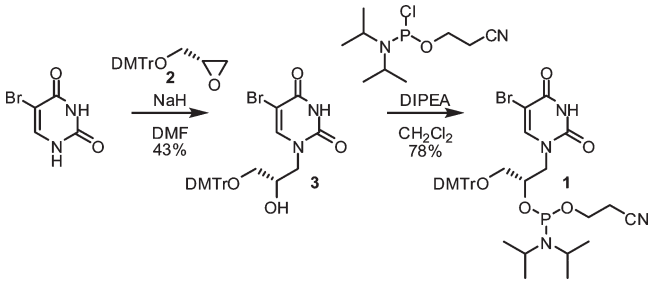

Figure 7. Synthesis of the phosphoramidite **1**.

affect previously studied nucleic acids, even though other explanations, e.g., different ion strengths, can currently not be excluded.[37] In conclusion, the combined effort of theory and experiment has shed light on both the structure and inherent thermodynamic stability and dynamics of unmodified GNA. The discovery of a pronounced twisting/untwisting mode of dsGNA could not only play an important role in the high thermodynamic stability of GNA but also give a hint as to why the simplest form of a duplex-forming nucleic acid currently known was not chosen by life. Obviously, the large degree of backbone variations would hamper trivial modes of sequence-specific recognition by biological macromolecules.

EXPERIMENTAL SECTION

Synthesis of the 5-Bromouracil Phosphoramidite for Automated Solid-Phase Synthesis. *General Procedures and Reagents.* NMR spectra were recorded on a 300 MHz spectrometer. High-resolution mass spectra were obtained with a LTQ-FT instrument using ES ionization. Reactions were performed under an atmosphere of argon unless otherwise specified. Compound **2** was prepared as described previously[43] and its identity and purity were confirmed using ^{1}H NMR.

*Compound **3***. To a suspension of 5-bromouracil (1.04 g, 5.5 mmol) in anhydrous DMF (11 mL) under argon was added NaH (44 mg, 1.1 mmol, 60% in mineral oil) and the solution was allowed to stir under argon for 1 h. A solution of compound **2** (1.95 g, 5.2 mmol) in DMF (11 mL) was added to the first solution and then heated to 85 °C overnight. The next morning, the solution was cooled, all solvent removed, and the resulting oil coevaporated with toluene, redissolved in ethyl acetate, and concentrated again. The product was purified via flash chromatography over silica gel starting with 2:1:0.01 hexanes:acetone:Et_3N, then 3:2:0.01 hexanes:acetone:Et_3N, and finally eluting with 1:1:0.01 hexanes:acetone:Et_3N to afford compound **3** as a white foam (1.32 g, 43%). ^{1}H NMR (300 MHz, $CDCl_3$) δ (ppm): 7.65 (s, 1H), 7.46 (d, J = 7.4 Hz, 2H), 7.39−7.17 (m, 7H), 6.85 (d, J = 8.8 Hz, 4H), 4.14 (m, 2H), 3.79 (s, 6H), 3.64 (dd, J = 14.5, 8.6 Hz, 1H), 3.21 (d, J = 4.5 Hz, 2H). ^{13}C NMR (75 MHz, $CDCl_3$) δ (ppm): 160.0, 158.6, 151.0, 145.8, 144.6, 135.7, 130.0, 128.07, 128.01, 127.0, 113.3, 95.8, 86.5, 68.7, 64.6, 55.3, 52.3. IR (solid) ν (cm^{-1}): 3439 (br), 3168 (br), 3059, 2931, 2835, 1675, 1606, 1506, 1443, 1347, 1300, 1245, 1174, 1070, 1029, 906, 826, 727, 701, 621, 582, 526, 423. HRMS: calcd for $C_{28}H_{27}N_2O_6BrNa$ $(M + Na)^+$ 589.0945, found $(M + Na)^+$ 589.0956.

*Phosphoramidite **1***. To an argon-purged solution of compound **3** (1.00 g, 1.8 mmol) and *N*,*N*-diisopropylethylamine (1.85 mL, 10.6 mmol) in methylene chloride (30 mL) was added 2-cyanoethyl *N*,*N*-diisopropylchlorophosphoramidite (0.59 mL, 2.6 mmol) dropwise and the solution stirred for 2 h at room temperature under argon. The solution was diluted with methylene chloride and washed once with saturated aqueous $NaHCO_3$, dried over Na_2SO_4, and finally concentrated. The crude product was purified by flash chromatography over silica gel using 3:2:0.01 hexanes:acetone:Et_3N to afford phosphoramidite **1** (see Figure 7) as a white foam (1.05 g, 78%). ^{31}P NMR (162 MHz, $CDCl_3$) δ (ppm): 150.6, 150.2. HRMS: calcd for $C_{37}H_{45}N_4O_7BrP$ $(M + H)^+$ 767.2204, found $(M + H)^+$ 767.2206.

GNA Oligonucleotide Synthesis and Purification. GNA oligonucleotides were prepared by an DNA/RNA synthesizer on a 1 μmol scale. GNA phosphoramidites were used at a concentration of 100 mM with a standard protocol for 2-cyanoethyl phosphoramidites, except that the coupling was extended to 3 min. After the trityl-on synthesis, the resin was incubated with concentrated aqueous ammonia at room temperature overnight in the dark. The entire solution was then applied directly to a Sep-Pak Classic reverse phase column (Waters, 360 mg) and washed sequentially with 3% NH_4OH (15 mL), water (10 mL), 1.5% aqueous TFA (10 mL), and water (10 mL), and the oligonucleotides finally eluted with 20% aqueous acetonitrile. The oligonucleotides were further purified by HPLC eluting over a Waters Xterra column (MS C_{18}, 4.6 × 50 mm, 2.5 μM particle size) at 60 °C with a linear gradient (flow = 1.0 mL/min) of acetonitrile and aqueous triethylammonium acetate buffer (50 mM, pH = 7.0). Identities were confirmed by MALDI-TOF MS.

X-ray Crystallography. The 8-mer-BrGNA duplex used for structural analysis had the sequence 3′-CTC^{Br}UAGAG-2′, where the 5-bromouracil at position 4 allowed phasing by multiple anomalous dispersion (MAD) at the bromine edge. The 8-mer-BrGNA duplex gave rodlike crystals in sitting-drop setups after 2 weeks at 4 °C in 10% 2-methyl-2,4-pentanediol, 40 mM sodium cacodylate, pH 5.5, 20 mM cobalt hexamine, 40 mM LiCl, 20 mM $MgCl_2$. Accordingly, MAD diffraction data up to a resolution of 1.8 Å were recorded at synchrotron beamline ID23-1, ESRF, Grenoble. After data reduction and scaling the crystal structure was solved by SHELXE in the tetragonal space group $I4_122$ ($a = b$ = 56.93 Å, c = 28.97 Å) and refined by alternating cycles of REFMAC5[44] and COOT[45] using stereochemical parameters derived from the previously determined atomic resolution structure of a 6-mer-BrGNA duplex. Given the data quality, structure refinement with one molecule per asymmetric symmetry unit converged at apparently rather high but acceptable *R*-factor/*R*-free values of 23.4%/27.1%. Indexing and refinement of the 8-mer-BrGNA duplex structure was repeated in alternative, lower symmetry space groups, but that did not alleviate this problem. Closer inspection of the difference electron density indicated helical but distorted features in the intervening, large solvent channels (calculated solvent content 65%). These density features might correspond to GNA duplexes highly disordered in the crystal lattice and were hence not amenable for structural modeling. The asymmetric unit of the refined GNA duplex structure contains one single strand, 19 H_2O molecules, and two Na^+ ions. The 3′-terminal cytosine nucleotide is partly disordered as indicated by an occupancy of only 70%.

Computational Methodology. The sequences of GNA shown in Table 1 were built starting from the X-ray structures of the hydroxypyridone copper complex[15] or the bromo-GNA structures in *xleap*. Charges for all GNA nucleosides were derived using RESP fitting on DFT-optimized and modified GNA residues. Geometry optimizations were performed using Gaussian 03[46] at the B3LYP/6-31G* level while the backbone torsional angles were restrained to those found in the experimentally observed structure. Electrostatic potentials were calculated at the HF/6-31G* level of theory by fitting of the RESP charges using *antechamber* and setting intermolecular equivalencies as needed.[47] All MD simulations and postprocessing was performed using the AMBER 9 suite of programs[48], and in analogy to our previous studies of non-natural oligonucleotides, the structures were loaded into *xleap* and edited as needed.[23−26]

For simulations of natural nonmetalated GNA sequences the corresponding hydroxypyridone base pairs were removed and replaced with either A or T. This was done by removing the entire nucleobase except for the nitrogen linkage to the backbone and flanking carbons. Atoms

were then renamed to correspond to the new nucleobases, and *xleap* was allowed to automatically add in the missing atoms. Unlike the case of DNA and RNA, the effect of ion strength in MD simulations has not yet been studied in detail and only the number of Na^+ counterions necessary to balance the negative charge of the phosphate backbone were included in the simulation. Finally, the solute was placed in a pre-equilibrated box of TIP3P waters extending 8 Å beyond the solute in each dimension. Table 1 provides the sequences of all the nucleic acids studied (AMBER atom types used for the GNA backbone can be found in Figure S9 in the Supporting Information). 16-mer-GNA, 16-mer-CuGNA, and 16-mer-BrGNA were built by including an additional duplex from the crystal structure. PyMol 0.99 was used to generate symmetry-mates and retain an additional duplex stacked end to end against the original 8-mer structure as well as to generate the figures. These quasi-continuous forms were then subsequently edited as described above. All starting geometries and additional instructions on how to perform these simulations are available in the Supporting Information.

After the initial setup was complete, minimization was performed first by restraining the solute and allowing sodium ions and water to relax. For the case of unmodified GNAs, an additional minimization step was included where restraints were added between hydrogen bonds of the replaced nucleotides. Finally, the entire system was allowed to relax prior to the MD simulations. The particle mesh Ewald molecular dynamics (*pmemd*) module of AMBER 9 was used to perform all MD simulations in order to increase the efficiency of the parallel simulations. Parameters for the simulations were adopted from the Cornell et al. forcefield, along with the adjustments by Wang et al. (Parm99).[49,50] A bonded model was used to describe the base pairs in the hydroxypyridone−copper complex, and parameters were fit to reproduce the coordinates from the crystal structure. Equilibration and heating of the system including the GNA and a water box as shown in Figure S4 (Supporting Information) was performed using a constant volume (*NVT*) ensemble by adding a 10 kcal mol^{-1} restraint on the solute while the system was heated from 0 to 300 K over 20 ps. Solute restraints are then removed and the system is equilibrated for 200 ps in a constant pressure (*NPT*) ensemble at 1 atm. Production runs of 20 ns (100 ns for 16-mer-GNA) were subsequently performed. Two femtosecond time steps were used for DNA, GNA, and BrGNA while 1 fs time steps were required for system stability in the hydroxypyridone GNA examples. SHAKE was used in all simulations to restrain bonds to hydrogen.

Parameters for unmodified GNA bases and glycol backbone were taken directly from the Cornell et al. force field.[49] It should be noted that the crucial backbone torsional parameters in this force field were fit to reproduce experimental and quantum mechanical results for methyl ethyl ether and similar acyclic models. It therefore should be expected that this force field will perform quite well in describing the backbone parameters in GNA, as the backbone is actually more similar to the training sets used to create the force field than the more widely studied DNA is. A more limited study of GNA using the parameter set gave indeed results in excellent agreement with experiment.[31] To further test the applicability of the AMBER force field to GNA, MP2/6-31G* calculations of O−C−C−O torsional energies were compared to results using AMBER. Two model systems were used for this study, one for GNA and one for DNA. It is found that the AMBER force field performs similarly for both systems, successfully displaying that the force field is as effective in describing the backbone torsions present in GNA as well as what is observed in DNA.

Postprocessing was performed using the *ptraj* module of AMBER 9. C1′−C1′ intrastrand distances, P−P intrastrand distances, and all hydrogen-bond distances were extracted for analysis. Structures were extracted every 20 ps to give a total of 1000 structures per simulation. Curves 5.1 was then used to calculate the helical parameters for each pdb and results were either averaged or viewed over time.[33,34]

Structures of the model systems used and graphs of the torsional energies can be found in the Supporting Information.

■ ASSOCIATED CONTENT

Supporting Information. Details of the X-ray crystallographic and computational studies as well as analytical information. This material is available free of charge via the Internet at http://pubs.acs.org. The coordinates and structure factors of 8-mer-BrGNA are deposited in the RCSB database under accession code 2XC6.

■ AUTHOR INFORMATION

Corresponding Author

*E-mail: owiest@nd.edu, essen@chemie.uni-marburg.de, meggers@chemie.uni-marburg.de.

■ ACKNOWLEDGMENT

We would like to thank the Center of Research Computing at the University of Notre Dame and Teragrid (Grant CHE090124) for the generous allocation of computer resources used in this project. We also gratefully acknowledge a Peter J. Grace Fellowship from the University of Notre Dame to A.T.J. The authors thank Sandor Brockhauser for support at ESRF beamline ID23-1, Grenoble, and the reviewers for valuable suggestions.

■ REFERENCES

(1) Watson, J. D.; Crick, F. H. C. *Nature* **1953**, *171*, 737.
(2) Appella, D. H. *Curr. Opin. Chem. Biol.* **2009**, *13*, 687.
(3) Schneider, K. C.; Benner, S. A. *J. Am. Chem. Soc.* **1990**, *112*, 453.
(4) Azymah, M.; Chavis, C.; Lucas, M.; Morvan, F.; Imbach, J. L. *Nucleosides Nucleotides* **1992**, *11*, 1241.
(5) Vandendriessche, F.; Augustyns, K.; Vanaerschot, A.; Busson, R.; Hoogmartens, J.; Herdewijn, P. *Tetrahedron* **1993**, *49*, 7223.
(6) Nielsen, P.; Kirpekar, F.; Wengel, J. *Nucleic Acids Res.* **1994**, *22*, 703.
(7) Nielsen, K. D.; Kirpekar, F.; Roepstorff, P.; Wengel, J. *Bioorg. Med. Chem.* **1995**, *3*, 1493.
(8) Peng, L.; Roth, H. J. *Helv. Chim. Acta* **1997**, *80*, 1494.
(9) Eschenmoser, A. *Science* **1999**, *284*, 2118.
(10) Schoning, K. U.; Scholz, P.; Guntha, S.; Wu, X.; Krishnamurthy, R.; Eschenmoser, A. *Science* **2000**, *290*, 1347.
(11) Wippo, H.; Reck, F.; Kudick, R.; Ramaseshan, M.; Ceulemans, G.; Bolli, M.; Krishnamurthy, R.; Eschenmoser, A. *Bioorg. Med. Chem.* **2001**, *9*, 2411.
(12) Zhang, L.; Peritz, A.; Meggers, E. *J. Am. Chem. Soc.* **2005**, *127*, 4174.
(13) Schlegel, M. K.; Peritz, A. E.; Kittigowittana, K.; Zhang, L.; Meggers, E. *Chembiochem* **2007**, *8*, 927.
(14) Schlegel, M. K.; Xie, X.; Zhang, L.; Meggers, E. *Angew. Chem. Int. Ed.* **2009**, *48*, 960.
(15) Schlegel, M. K.; Essen, L.-O.; Meggers, E. *J. Am. Chem. Soc.* **2008**, *130*, 8158.
(16) Schlegel, M. K.; Essen, L.-O.; Meggers, E. *Chem. Commun.* **2010**, *46*, 1094.
(17) Schlegel, M. K.; Xie, X.; Zhang, L.; Meggers, E. *Angew. Chem. Int. Ed.* **2009**, *48*, 960.
(18) Cheatham, T. E.; Kollman, P. A. *Annu. Rev. Phys. Chem.* **2000**, *51*, 435.
(19) Cheatham, T. E.; Srinivasan, J.; Case, D. A.; Kollman, P. A. *J. Biomol. Struct. Dyn.* **1998**, *16*, 265.
(20) Seibel, G. L.; Singh, U. C.; Kollman, P. A. *Proc. Natl. Acad. Sci. U. S. A.* **1985**, *82*, 6537.
(21) Dixit, S. B.; Beveridge, D. L.; Case, D. A.; Cheatham, T. E.; Giudice, E.; Lankas, F.; Lavery, R.; Maddocks, J. H.; Osman, R.; Sklenar, H.; Thayer, K. M.; Varnai, P. *Biophys. J.* **2005**, *89*, 3721.

(22) Orozco, M.; Noy, A.; Perez, A. *Curr. Opin. Struct. Biol.* **2008**, *18*, 185.
(23) O'Daniel, P. I.; Jefferson, M.; Wiest, O.; Seley-Radtke, K. L. *J. Biomol. Struct. Dyn.* **2008**, *26*, 283.
(24) O'Neil, L. L.; Grossfield, A.; Wiest, O. *J. Phys. Chem. B* **2007**, *111*, 11843.
(25) O'Neil, L. L.; Wiest, O. *J. Phys. Chem. B* **2008**, *112*, 4113.
(26) O'Neil, L. L.; Wiest, O. *Org. Biomol. Chem.* **2008**, 6.
(27) Ivanova, A.; Rosch, N. *J. Phys. Chem. A* **2007**, *111*, 9307.
(28) He, W.; Hatcher, E.; Balaeff, A.; Beratan, D. N.; Gil, R. R.; Madrid, M.; Achim, C. *J. Am. Chem. Soc.* **2008**, *130*, 13264.
(29) Lynch, S. R.; Liu, H. B.; Gao, J. M.; Kool, E. T. *J. Am. Chem. Soc.* **2006**, *128*, 14704.
(30) De Winter, H.; Lescrinier, E.; Van Aerschot, A.; Herdewijn, P. *J. Am. Chem. Soc.* **1998**, *120*, 5381.
(31) Zhou, H.; Johnson, A. T.; Wiest, O.; Zhang, L. *Org. Biomol. Chem.* **2011**, *13*, 2840.
(32) Olson, W. K.; Zhurkin, V. B. *Curr. Opin. Struct. Biol.* **2000**, *10*, 286.
(33) Lavery, R.; Sklenar, H. *J. Biomol. Struct. Dyn.* **1988**, *6*, 63.
(34) Lavery, R.; Sklenar, H. *J. Biomol. Struct. Dyn.* **1989**, *6*, 655.
(35) Olson, W. K.; Bansal, M.; Burley, S. K.; Dickerson, R. E.; Gerstein, M.; Harvey, S. C.; Heinemann, U.; Lu, X.; Neidle, S.; Shakked, Z.; Sklenar, H.; Suzuki, M.; Tung, C. S.; Westhof, E.; Wolberger, C.; Berman, H. M. *J. Mol. Biol.* **2001**, *313*, 229.
(36) Johannsen, S.; Megger, N.; Böhme, D.; Sigel, R. K. O.; Müller, J. *Nat. Chem.* **2010**, *2*, 229.
(37) Bevan, D. R.; Li, L. P.; Pedersen, L. G.; Darden, T. A. *Biophys. J.* **2000**, *78*, 668.
(38) Mura, C.; McCammon, J. A. *Nucleic Acids Res.* **2008**, *36*, 4941.
(39) Li, L.; Uversky, V. N.; Dunker, A. K.; Meroueh, S. O. *J. Am. Chem. Soc.* **2007**, *120*, 15668.
(40) Johnson, A. T.; Wiest, O. *J. Phys. Chem. B* **2007**, *111*, 14398.
(41) Girard, E.; Prange, T.; Dhaussy, A.-C.; Migianu-Griffoni, E.; Lecouvey, M.; Chervin, J.-C.; Mezouar, M.; Kahn, R.; Fourme, R. *Nucleic Acids Res.* **2007**, *35*, 4000.
(42) Bomble, Y. J.; Case, D. A. *Biopolymes* **2008**, *89*, 722.
(43) Zhang, L.; Peritz, A. E.; Carroll, P. J.; Meggers, E. *Synthesis* **2006**, 645.
(44) Collaborative Computing Project Number 4 *Acta Crystallog. Sect. D* **1994**, *50*, 760.
(45) Emsley, P.; Cowtan, K. *Acta Crystallogr. Sect. D* **2004**, *60*, 2126.
(46) Frisch, M. J.; Trucks, G. W.; Schlegel, H. B.; Scuseria, G. E.; Robb, M. A.; Cheeseman, J. R.; Montgomery, J. A., Jr.; Vreven, T.; Kudin, K. N.; Burant, J. C.; Millam, J. M.; Iyengar, S. S.; Tomasi, J.; Barone, V.; Mennucci, B.; Cossi, M.; Scalmani, G.; Rega, N.; Petersson, G. A.; Nakatsuji, H.; Hada, M.; Ehara, M.; Toyota, K.; Fukuda, R.; Hasegawa, J.; Ishida, M.; Nakajima, T.; Honda, Y.; Kitao, O.; Nakai, H.; Klene, M.; Li, X.; Knox, J. E.; Hratchian, H. P.; Cross, J. B.; Bakken, V.; Adamo, C.; Jaramillo, J.; Gomperts, R.; Stratmann, R. E.; Yazyev, O.; Austin, A. J.; Cammi, R.; Pomelli, C.; Ochterski, J. W.; Ayala, P. Y.; Morokuma, K.; Voth, G. A.; Salvador, P.; Dannenberg, J. J.; Zakrzewski, V. G.; Dapprich, S.; Daniels, A. D.; Strain, M. C.; Farkas, O.; Malick, D. K.; Rabuck, A. D.; Raghavachari, K.; Foresman, J. B.; Ortiz, J. V.; Cui, Q.; Baboul, A. G.; Clifford, S.; Cioslowski, J.; Stefanov, B. B.; Liu, G.; Liashenko, A.; Piskorz, P.; Komaromi, I.; Martin, R. L.; Fox, D. J.; Keith, T.; Al-Laham, M. A.; Peng, C. Y.; Nanayakkara, A.; Challacombe, M.; Gill, P. M. W.; Johnson, B.; Chen, W.; Wong, M. W.; Gonzalez, C.; Pople, J. A. *Gaussian 03*; Gaussian: Wallingford, CT, 2004.
(47) Cieplak, P.; Cornell, W. D.; Bayly, C.; Kollman, P. A. *J. Comput. Chem.* **1995**, *16*, 1357.
(48) Case, D. A.; Darden, T. A.; Cheatham, T. E., III; Simmerling, C. L.; Wang, J.; Duke, R. E.; Luo, R.; Merz, K. M.; Pearlman, D. A.; Crowley, M.; Walker, R. C.; Zhang, W.; Wang, B.; Hayik, S.; Roitberg, A.; Seabra, G.; Wong, K. F.; Paesani, F.; Wu, X.; Brozell, S.; Tsui, V.; Gohlke, H.; Tan, C.; Mongan, J.; Hornak, V.; Cui, G.; Beroza, P.; Mathews, D. H.; Schafmeister, C.; Ross, W. S.; Kollman, P. A. *AMBER 9*; University of California: San Francisco, 2006.
(49) Cornell, W. D.; Cieplak, P.; Bayly, C. I.; Gould, I. R.; Merz, K. M.; Ferguson, D. M.; Spellmeyer, D. C.; Fox, T.; Caldwell, J. W.; Kollman, P. A. *J. Am. Chem. Soc.* **1995**, *117*, 5179.
(50) Wang, J. M.; Cieplak, P.; Kollman, P. A. *J. Comput. Chem.* **2000**, *21*, 1049.